THE JOURNAL OF BIOLOGICAL CHEMISTRY VOL. 287, NO. 4, pp. 2706–2718, January 20, 2012

Regulation of Peroxisomal Lipid Metabolism by Catalytic Activity of Tumor Suppressor H-rev107*

Received for publication, June 2, 2011, and in revised form, November 27, 2011 Published, JBC Papers in Press, December 1, 2011, DOI 10.1074/jbc.M111.267575

Toru Uyama[‡], Ikuyo Ichi[§], Nozomu Kono[§¶], Asuka Inoue[‖], Kazuhito Tsuboi[‡], Xing-Hua Jin[‡], Nobukazu Araki[**], Junken Aoki[‖], Hiroyuki Arai[§¶], and Natsuo Ueda[‡1]

From the Departments of [‡]Biochemistry and [**]Histology and Cell Biology, Kagawa University School of Medicine, 1750-1 Ikenobe, Miki, Kagawa 761-0793, Japan, the [§]Graduate School of Pharmaceutical Sciences, University of Tokyo, Tokyo 113-0033, Japan, [¶]Core Research for Evolutional Science and Technology (CREST), Japan Science and Technology Agency, Kawaguchi, Saitama 332-0012, Japan, and the [‖]Graduate School of Pharmaceutical Sciences, Tohoku University, Miyagi 980-8578, Japan

Background: Physiological function of the tumor suppressor H-rev107, showing a phospholipase $A_{1/2}$ activity, is poorly understood.
Results: Overexpression of the catalytically active H-rev107 in mammalian cells decreased endogenous levels of ether-type lipids and altered intracellular localization of peroxisomal markers.
Conclusion: H-rev107 may enzymatically regulate peroxisomal function.
Significance: These results suggest a physiological role of H-rev107 discovered as a tumor suppressor.

H-rev107 is a mammalian protein belonging to the HRAS-like suppressor family. Although the protein was originally found as a tumor suppressor, currently it is receiving considerable attention as a regulator of adipocyte lipolysis. We recently revealed that purified recombinant H-rev107 has phospholipase $A_{1/2}$ activity, releasing free fatty acids from glycerophospholipids with a preference for esterolysis at the *sn*-1 position. In the present study, we constitutively expressed H-rev107 in cloned HEK293 cells to examine its biological function in living cells. Initially, the cells accumulated free fatty acids. We also found a remarkable decrease in the levels of ether-type lipids, including plasmalogen and ether-type triglyceride, with a concomitant increase in fatty alcohols, substrates for the biosynthesis of ether-type lipids. Considering that peroxisomes are involved in the ether-type lipid biosynthesis, we next focused on peroxisomes and found that the peroxisomal markers 70-kDa peroxisomal membrane protein and catalase were abnormally distributed in the transfected cells. These biochemical and morphological abnormalities were not seen in HEK293 cells stably expressing a catalytically inactive mutant of H-rev107. When H-rev107 or its fusion protein with enhanced green fluorescence protein was transiently expressed in mammalian cells, both proteins were associated with peroxisomes in some of the observed cells. These results suggest that H-rev107 interferes with the biosynthesis of ether-type lipids and is responsible for the dysfunction of peroxisomes in H-rev107-expressing cells.

In human beings, the HRAS-like suppressor (HRASLS)[2] family, or H-rev107 family, consists of five protein molecules (H-rev107, TIG3 (tazarotene-induced gene 3), A-C1, HRASLS2, and Ca^{2+}-independent *N*-acyltransferase) sharing a common structure (1, 2). H-rev107 is the first member of this family to be discovered and has been characterized as a type II tumor suppressor (3–5). However, we recently found that this protein shows phospholipase $A_{1/2}$ ($PLA_{1/2}$) activity for glycerophospholipids with a preference for hydrolysis at the *sn*-1 position of the glycerol backbone (6, 7). We also reported that other members of this family function as phospholipid-metabolizing enzymes (7–9). On the other hand, Duncan *et al.* (10) reported that H-rev107 is a novel PLA_2 enzyme with a preference for hydrolysis at the *sn*-2 position.

Notably, H-rev107 was highly expressed in adipose tissues, and its expression level in white adipose tissues in genetically obese *ob/ob* mice was much higher than that in wild-type mice (11). In addition, the expression level increased during the differentiation of 3T3-L1 cells, a mouse preadipocyte cell line (12). More recently, Jaworski *et al.* (11) generated *H-rev107*-deficient mice and showed that *H-rev107* ablation leads to marked reduction in adipose tissue mass and TG content despite the occurrence of normal adipogenesis. In the *H-rev107*-deficient mice, prostaglandin E_2 levels were decreased. Prostaglandin E_2 is generated from arachidonic acid and by binding to the $G\alpha_i$-coupled receptor EP3. The prostaglandin E_2-EP3 complex decreases cyclic AMP levels, resulting in the inactivation of lipolysis. Thus, it was suggested that H-rev107 stimulates the accumulation of lipid droplets by functioning as a PLA_2 that

* This work was supported by grants-in-aid for Scientific Research from the Ministry of Education, Culture, Sports, Science, and Technology of Japan (to T. U.) and the Japan Society for the Promotion of Science (to N. U.). This work was also supported by grants from the Kagawa University Faculty of Medicine Specially Promoted Research Fund 2010 (to T. U.), the Fund for Kagawa University Young Scientists 2011 (to T. U.), the Ichiro Kanehara Foundation (to T. U.), the Sumitomo Foundation (to T. U.), the Uehara Memorial Foundation (to T. U.), and Core Research for Evolutional Science and Technology (CREST) (to N. K. and H. A.).
[1] To whom correspondence should be addressed. Tel.: 81-87-891-2102; Fax: 81-87-891-2105; E-mail: nueda@med.kagawa-u.ac.jp.

[2] The abbreviations used are: HRASLS, HRAS-like suppressor; ADHAPS, alkyldihydroxyacetone phosphate synthase; DHAP, dihydroxyacetone phosphate; DHAPAT, dihydroxyacetone phosphate acyltransferase; ESI, electrospray ionization; EGFP, enhanced GFP; Far, fatty acyl-CoA reductase; PMP70, 70-kDa peroxisomal membrane protein; PC, phosphatidylcholine; PE, phosphatidylethanolamine; PLA, phospholipase A; PTS, peroxisomal targeting signal; TG, triglyceride; TG-E, ether-type triglyceride; ER, endoplasmic reticulum; MTT, 3-(4,5-dimethylthiazol-2-yl)-2,5-diphenyltetrazolium bromide.

releases arachidonic acid abundant in the *sn*-2 position of glycerophospholipids. However, because the dominant PLA_1 activity of H-rev107 was not considered, it was likely that H-rev107 has other physiological significance as a PLA_1 enzyme.

To elucidate the intracellular function of H-rev107, we established mammalian cells that stably express recombinant H-rev107. By using these cells we showed that H-rev107 acts as $PLA_{1/2}$ in living cells. More importantly, we found for the first time that the expression of H-rev107 causes a strong reduction in the levels of ether-type lipids, such as plasmalogen and ether-type triglyceride (TG-E). We also observed the dysfunction of peroxisomes where ether-type lipids are formed.

EXPERIMENTAL PROCEDURES

Materials—[1-^{14}C]Palmitic acid and 1,2-[1-^{14}C]dipalmitoyl-PC were purchased from PerkinElmer Life Sciences. [1-^{14}C]Hexadecanol was from Moravek Biochemicals (Brea, CA). Horseradish peroxidase-linked anti-mouse IgG, horseradish peroxidase-linked anti-rabbit IgG, Hybond P, and an ECL Plus kit were from GE Healthcare. 1,2-Dipalmitoyl-PC, 1-*O*-palmityl-2,3-dipalmitoyl-*rac*-glycerol, 1-hexadecanol, anti-actin, anti-H-rev107, and anti-70-kDa peroxisomal membrane protein (PMP70) monoclonal antibodies and anti-FLAG monoclonal antibody M2 were from Sigma. Dulbecco's modified Eagle's medium, Alexa 488-conjugated anti-rabbit IgG, Alexa 488-conjugated anti-mouse IgG, Lipofectamine 2000, Lipofectamine RNAiMAX, fetal calf serum, Geneticin, and pcDNA3.1(+) and pEF1/Myc-His vectors were from Invitrogen. An siRNA directed against mouse *H-rev107* and a control siRNA were obtained from B-Bridge International Inc. (Sunnyvale, CA). Antibodies against protein-disulfide isomerase, syntaxin 6, cytochrome *c* oxidase IV, and lamin A/C were from Cell Signaling Technology (Danvers, MA). Anti-catalase antibody was from Abcam Inc. (Cambridge, MA). pEnhanced green fluorescence protein-C1 (pEGFP-C1), pEGFP-N1, and pDsRed2-Peroxi vectors were from Clontech. Permafluor was from Immunotech (Marseille, France). Colorimetric MTT kit was from Millipore. The phospholipid C assay kit was from Wako Diagnostics (Osaka, Japan). Nonidet P-40 was from Nacalai Tesque, Inc. (Kyoto, Japan). *Ex Taq* DNA polymerase and PrimeScript RT reagent kit were from TaKaRa Bio Inc. (Ohtsu, Japan). The RNeasy minikit was from Qiagen. KOD-Plus DNA polymerase was from TOYOBO (Osaka, Japan). Anti-green fluorescence protein (GFP) antibody was from Medical and Biological Laboratories (Nagoya, Japan). Primulin was from Wako Pure Chemical Industries (Osaka, Japan). Protein assay dye reagent concentrate was from Bio-Rad, and precoated Silica Gel 60 F_{254} aluminum sheets (20 × 20 cm, 0.2 mm thick) for TLC were from Merck. HEK293 and HeLa cells were maintained in Dulbecco's modified Eagle's medium with 10% fetal calf serum at 37 °C in humidified air containing 5% CO_2.

Construction of Expression Vectors—Mouse brain cDNA was prepared from 5 μg of total RNA of mouse brain using Moloney murine leukemia virus reverse transcriptase and random hexamer. The cDNA encoding N-terminally FLAG-tagged mouse H-rev107 was amplified by PCR with the mouse brain cDNA as a template. The primers used were the forward primer 5′-CGCACTAGTGGAAAATGGATTACAAGGATGACGACGATAAGCTAGCACCCATACCAGAACCCAAG-3′ (Primer A), containing an SpeI site and an in-frame FLAG sequence, and the reverse primer 5′-CGCGCGGCCGCTCATTGCTTCTGTTTCTTGTTTC-3′ (Primer B), containing an NotI site. PCR was carried out with KOD-Plus DNA polymerase for 30 cycles at 94 °C for 20 s, 56 °C for 20 s, and 68 °C for 60 s in 5% (v/v) Me_2SO. The obtained DNA fragment was subcloned into the SpeI and NotI sites of pEF1/Myc-His. The cDNA for the catalytically inactive mutant H-rev107-C113S was prepared by megaprimer PCR, consisting of two sets of PCRs, using pEF1/Myc-His vector harboring mouse *H-rev107* as a template. An oligonucleotide 5′-GACCAGCGAGAACAGTGAGCACTTTGTGAA-3′ (the underline indicates the mismatch) and its complementary oligonucleotide were used as primers. Primers A and B were used as the forward primer and the reverse primer, respectively. In order to construct H-rev107 fused to the C terminus of EGFP (EGFP-H-rev107), another PCR was performed using pEF1/Myc-His vector harboring mouse *H-rev107* as a template. The primers used were the forward primer 5′-CGCGAATTCGATGCTAGCACCCATACCAGA-3′, containing an EcoRI site, and the reverse primer 5′-CGCGGATCCTCATTGCTTCTGTTTCTTGTTTCTG-3′, containing a BamHI site. The obtained DNA fragment was subcloned into the EcoRI and BamHI sites of pEGFP-C1. To construct H-rev107 fused to the N terminus of EGFP, PCR was performed using pEF1/Myc-His vector harboring mouse *H-rev107* as a template. The primers used were the forward primer 5′-CGCGAATTCGGAAAATGCTAGCACCCATACCAGAACCC-3′, containing an EcoRI site, and the reverse primer 5′-CGCGGATCCCCTTGCTTCTGTTTCTTGTTTCTG-3′ containing a BamHI site. The obtained DNA fragment was subcloned into the EcoRI and BamHI sites of pEGFP-N1. pcDNA3.1(+) vector harboring N-terminally FLAG-tagged rat *H-rev107* was prepared as described previously (6). All constructs were sequenced in both directions using an ABI 3130 Genetic Analyzer (Applied Biosystems Invitrogen).

Stable Expression of H-rev107 in Cells—HEK293 and CHO cells were transfected with pEF1/Myc-His vector harboring N-terminally FLAG-tagged mouse *H-rev107* or its mutant C113S or the insert-free pEF1/Myc-His vector by the use of Lipofectamine 2000. Cells were selected in the medium containing 1 mg/ml Geneticin. Clonal cell lines were isolated by colony lifting and maintained in the Geneticin-containing medium. To measure $PLA_{1/2}$ activity, the harvested cells were suspended in 20 mM Tris-HCl (pH 7.4) and sonicated three times each for 3 s. The cell homogenates (30 μg of protein) were incubated with 200 μM 1,2-[1-^{14}C]dipalmitoyl-PC (45,000 cpm) in 100 μl of 50 mM Tris-HCl (pH 8.0), 2 mM DTT, and 0.1% Nonidet P-40 at 37 °C for 30 min. The reaction was terminated with the addition of 320 μl of a mixture of chloroform/methanol (2:1, v/v) containing 5 mM 3(2)-*t*-butyl-4-hydroxyanisole. After centrifugation, 100 μl of the lower fraction was spotted on a silica gel thin layer plate (10-cm height) and developed at 4 °C for 25 min in chloroform/methanol/H_2O (65:25:4, v/v/v) (solvent A). The distribution of radioactivity on the plate was quantified using a BAS1500 bioimaging analyzer (FUJIX Ltd., Tokyo). The protein concentration was determined by the method of Bradford with BSA as a standard. For the MTT assay,

cells were plated on 96-well plates, each containing 100 μl of Dulbecco's modified Eagle's medium with 10% fetal calf serum. The plates were incubated at 37 °C in humidified air containing 5% CO_2. Cell viability was determined based on mitochondrial conversion of MTT to formazan. Absorbance at 570 nm was measured at 24 and 48 h after plating.

RNA Interference—To decrease the expression level of H-rev107, siRNAs were introduced into H-rev107/HEK293 cells with Lipofectamine RNAiMAX according to the manufacturer's instruction. The final concentration of siRNA was 15 nM. Forty-eight h after transfection, RT-PCR, $PLA_{1/2}$ assay, and metabolic labeling with [^{14}C]hexadecanol were performed.

Western Blotting—Samples were separated by SDS-PAGE and electrotransferred to a hydrophobic polyvinylidene difluoride membrane (Hybond P). The membrane was blocked with PBS containing 5% dried milk and 0.1% Tween 20 (buffer A) and then incubated with primary antibodies (1:2,000 dilution) in buffer A at room temperature for 1 h, followed by incubation with horseradish peroxidase-labeled secondary antibodies (1:4,000 dilution) in buffer A at room temperature for 1 h. Proteins were finally treated with an ECL Plus kit and visualized with the aid of a LAS1000plus lumino-imaging analyzer (FUJIX Ltd.).

Sucrose Density Gradient Centrifugation—Sucrose density gradient centrifugation was performed as described previously (13). The cells harvested from three 150-mm dishes were homogenized in 1.3 ml of 3 mM imidazole-HCl (pH 7.4) containing 0.25 M sucrose and 1 mM EDTA by a Teflon homogenizer, and the homogenates were centrifuged at 3,000 × *g* for 10 min to remove nuclei and heavy mitochondria. The resultant supernatants were centrifuged at 18,000 × *g* for 15 min to prepare light mitochondrial fractions (18,000 × *g* pellet). The supernatants were further centrifuged at 105,000 × *g* for 55 min to prepare microsomal fractions (105,000 × *g* pellets) and cytosolic fractions (105,000 × *g* supernatants). The light mitochondrial fractions were suspended in 0.5 ml of 3 mM imidazole-HCl (pH 7.4) containing 0.25 M sucrose and 1 mM EDTA and layered on a sucrose gradient (1.7 ml of 53.9% (w/w), 2.7 ml of 45.8%, 2.4 ml of 37.4%, and 1.7 ml of 23.2% from the bottom) and centrifuged at 120,000 × *g* for 3 h with an RPS40T swing rotor (Hitachi). Every 1-ml fraction was collected in nine tubes from the bottom and analyzed by Western blotting together with the homogenates and microsomal and cytosolic fractions.

RT-PCR—Total RNAs were isolated from cells using an RNeasy minikit. cDNAs were prepared from 1 μg of total RNA using a PrimeScript RT reagent kit and subjected to PCR amplification by *Ex Taq* DNA polymerase. The forward and reverse primers used were as follows: mouse H-rev107, 5′-GCTGACCAGCGAGAACTGTGAGCAC-3′ and 5′-CTCCAGCGATGCCTACCGCCTTGAC-3′ (nucleotides 476–500 and 555–579, respectively, in GenBank™ accession number NM_139269); human DHAPAT, 5′-GCAGCAGGAATGGACTTCCTGGGAATG-3′ and 5′-CTTCGAGGAAAAATTCAACAGGAGCATAAC-3′ (nucleotides 762–788 and 907–936 in NM_014236); human ADHAPS, 5′-GAGTACCAATGAGTGCAAAGCGCGGAGAG-3′ and 5′-CCCATCCATTCCATTTCATAACTTCTTGC-3′ (nucleotides 206–234 and 308–336 in NM_003659); human Far 1, 5′-TGAGGCAGAAAGCTGGACAGACACC-3′ and 5′-CGCTGTTGATTGCTATAATTTTCTC-3′ (nucleotides 286–310 and 384–408 in NM_032228); human Far 2, 5′-TTGTGAGGCCCAAGGCTGGCCAGAC-3′ and 5′-CTCTGATCTTCTCATGCACATTTGG-3′ (nucleotides 396–420 and 485–509 in NM_018099); human PMP70, 5′-GTCATTGTCGAAAGGTTGGCATCAC-3′ and 5′-AGTTGCCTCTGCCATCCATATGCAG-3′ (nucleotides 1934–1958 and 2011–2035 in NM_002858); human catalase, 5′-AAGGTTTGGCCTCACAAGGACTACCCTC-3′ and 5′-TAGGCAAAAAGGCGGCCCTGAAGCATTTTG-3′ (nucleotides 990–1017 and 1133–1162 in NM_001752); human GAPDH, 5′-CGCTGAGTACGTCGTGGAGTCCACT-3′ and 5′-AGCAGAGGGGGCAGAGATGATGACC-3′ (nucleotides 375–399 and 456–480 in NM_002046). The PCR conditions used were as follows: denaturation at 96 °C for 20 s, annealing at 60 °C for 20 s, and extension at 72 °C for 20 s (28 cycles).

TLC Analysis—For metabolic labeling, cells were grown at 37 °C to 80% confluence in a 100-mm dish containing Dulbecco's modified Eagle's medium with 10% fetal calf serum and were labeled with [1-^{14}C]hexadecanol (1.6 μCi) or [1-^{14}C]palmitic acid (1.6 μCi) for 18 h. Cells were then harvested and washed two times with PBS. The total lipids were extracted by the method of Bligh and Dyer (14), spotted on a silica gel thin layer plate (20-cm height), and developed at 4 °C for 1 h in solvent A or hexane/diethyl ether/acetic acid (75:25:1, v/v/v) (solvent B). The distribution of radioactivity on the plate was quantified using a BAS1500 bioimaging analyzer. For analysis of non-radiolabeled lipids, total lipids were extracted from cells grown in seven 150-mm dishes with acetone or by the method of Bligh and Dyer (14) and separated by TLC with solvent A or B. Lipids were then visualized with 0.005% primulin under ultraviolet light (360 nm).

LC-ESI/MS Analysis—The lipids of cultured cells were extracted by the method of Bligh and Dyer (14). To degrade plasmenylethanolamine, the cells were treated with 5% trichloroacetic acid (TCA) for 30 min, followed by total lipid extraction. Mass spectrometry (MS) analysis was performed as described previously by using a Quattro Micro tandem quadrupole mass spectrometer (Waters) equipped with an electrospray ionization (ESI) source (15). Phospholipid molecular species were separated and analyzed using normal phase liquid chromatography ESI-MS with a Deverosil Si60 silica column (150 × 0.3-mm inner diameter, 5-μm particle size, Nomura Chemicals, Nagoya, Japan). The samples were provided by an UltiMate high performance liquid chromatography system (Dionex Corp.) into the electrospray interface at a flow rate of 4 μl/min. For both positive and negative ionization, the mobile phase consisted of acetonitrile/methanol (2:1) containing 0.1% ammonium formate (pH 6.4) (solvent C) and methanol/water (2:1) containing 0.1% ammonium formate (pH 6.4) (solvent D). The mobile phase was started with 100% acetonitrile. After 5 min, the mobile phase was changed from 100% acetonitrile to a mixture of solvent C and D (90:10). The linear gradient reached 40% solvent C at 20 min. The mobile phase was then held constant for 15 min. Nitrogen was used as drying gas. Desolvation gas flow was 523 liters/h, and cone gas flow was maintained at 42 liters/h. Desolvation temperature was 150 °C, and source temperature was 90 °C. The capillary and cone voltages were set

at 3.4–3.7 kV and 36–40 V, respectively. Argon was used as collision gas for collision-associated dissociation experiments at a pressure of 5×10^{-4} millibars. The collision energy was set to 40 eV for all collision-associated dissociation experiments. To form lithiated adducts of PC species, lithium acetate was added to solvent C and D at a concentration of 20 mM. The molecular species of each phospholipid class was quantified by comparisons of individual ion peak intensity with dimyristoyl-PE and dimyristoleoyl-PC as internal standards.

Analysis of Lysophospholipids by LC-MS/MS—Cells were homogenized in methanol. The obtained homogenates were centrifuged at 21,500 × *g* for 10 min, and the resultant supernatants were recovered. Concentration of choline-containing phospholipid was determined using a phospholipid C assay kit. Injection samples were prepared at 100 μM of methanol-extracted phospholipid mixed with internal standards, 17:0-lysophosphatidic acid, and 17:0-lyso-PC, at 1 μM. Ten μl of injection samples were analyzed by a standard LC-MS/MS method. Briefly, lysophospholipids were separated by Nanospace LC (Shiseido, Tokyo, Japan) with a C18 CAPCELL PAK ACR column (Shiseido), using a gradient of water containing 5 mM ammonium formate and 95% (v/v) acetonitrile containing 5 mM ammonium formate and then analyzed by MS/MS using a Quantum Ultra triple quadrupole mass spectrometer (Thermo Fisher Scientific). Lyso-PC was monitored in the positive ion mode, and other lysophospholipids were monitored in the negative ion mode.

GC/MS Analysis—Isolated lipids were methylated with 2.5% H_2SO_4 in methanol. The resulting fatty acid methyl esters were then extracted with hexane and quantitated by GC/MS analysis using an Agilent 7890A-5975C GC/MS network system (Agilent Technologies, Wilmington, DE) equipped with a DB-23 capillary column (60 m × 0.25 mm × 0.15 μm; Agilent Technologies) using heptadecanoic acid (17:0) as an internal standard. In the oven temperature program, the temperature was initiated at 50 °C for 1 min and then raised to 175 °C at 25 °C/min and to 235 °C at 5 °C/min and held for 5 min. The injector and detector temperatures were at 250 °C.

Microscopy—Cells were plated onto glass bottom plates and transiently transfected with pDsRed2-Peroxi vector and/or pEGFP-C1 vector harboring *H-rev107*. Forty-eight h after transfection, the cells were placed in Ringer's buffer in a temperature-controlled chamber at 37 °C and observed with a TE300 epifluorescence microscope (Nikon, Tokyo, Japan) (16). Fluorescent images of live cells were then captured using a cooled CCD camera controlled by the MetaMorph imaging system (Universal Imaging Corp., West Chester, PA). Some specimens were observed with an LSM 700 confocal laser microscope (Carl Zeiss).

Immunocytochemistry—For immunocytochemistry, cells were cultured on 12-mm glass coverslips containing Dulbecco's modified Eagle's medium with 10% fetal calf serum. The cells were then fixed with 4% paraformaldehyde in 0.1 M phosphate buffer (pH 7.4) for 10 min. The fixed cells were rinsed in PBS and treated with 0.25% NH_4Cl in PBS for 10 min to quench free aldehyde groups. The cells were then washed with PBS and permeabilized with 0.25% Triton X-100 in PBS for 10 min. After treatment with a blocking buffer (5% BSA in PBS) for 1 h, the cells were incubated with antibodies against PMP70 (2 μg/ml), catalase (1:300 dilution), or H-rev107 (1:100 dilution) in 1% BSA/PBS for 1 h at room temperature. The cells were washed with PBS and labeled with Alexa 488-conjugated anti-rabbit IgG (1:1,000 dilution) in PBS for 1 h. The specimen coverslips were mounted on glass slides using the mounting medium Permafluor and were observed with an LSM 700 confocal laser microscope. The signals of Alexa 488 were detected with excitation at 488 nm.

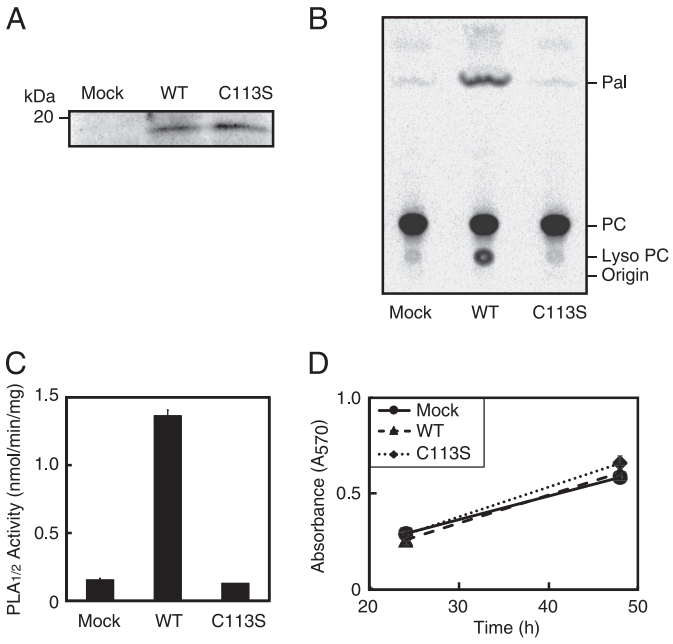

FIGURE 1. **Stable expression of H-rev107 in HEK293 cells.** Homogenates (30 μg of protein) of Mock/HEK293 (*Mock*), H-rev107/HEK293 (*WT*), and C113S/HEK293 cells (*C113S*) were analyzed by Western blotting with anti-FLAG antibody (*A*) or were subjected to the $PLA_{1/2}$ assay with 200 μM 1,2-[^{14}C]dipalmitoyl-PC as a substrate (*B* and *C*). The products were separated by TLC with solvent A (*B*), and $PLA_{1/2}$ activity was quantified (mean values ± S.D., $n = 3$) (*C*). The positions of authentic compounds on the TLC plate are indicated. *Pal*, palmitic acid. *D*, Mock/HEK293 (*solid line*), H-rev107/HEK293 (*dashed line*), and C113S/HEK293 (*dotted line*) cells were plated at equal numbers (2×10^4 cells), and their growth was examined by an MTT assay (mean values ± S.D. (*error bars*), $n = 3$).

RESULTS

Establishment of HEK293 Cells Stably Expressing H-rev107—To examine the role of H-rev107 in living cells, we cloned an HEK293 cell that stably expressed N-terminally FLAG-tagged mouse H-rev107 under the control of human elongation factor 1α-subunit promoter (H-rev107/HEK293 cell). We also established an HEK293 cell clone that expressed a catalytically inactive point mutant of H-rev107 (C113S/HEK293 cell). In this mutant, cysteine 113, which forms the Cys-His-His catalytic triad (17), was substituted with serine. Stable expression of the wild-type H-rev107 and the C113S mutant was confirmed by Western blotting, which gave immunopositive bands with the expected molecular masses (~19 kDa) (Fig. 1*A*). Judging from the intensities of the bands, the expression levels of both proteins appeared similar to each other. We next examined $PLA_{1/2}$ activity of the cell homogenates using [^{14}C]dipalmitoyl-PC as a substrate, which was labeled with ^{14}C on both 1-*O*-palmitoyl and 2-*O*-palmitoyl chains. When the products were analyzed by

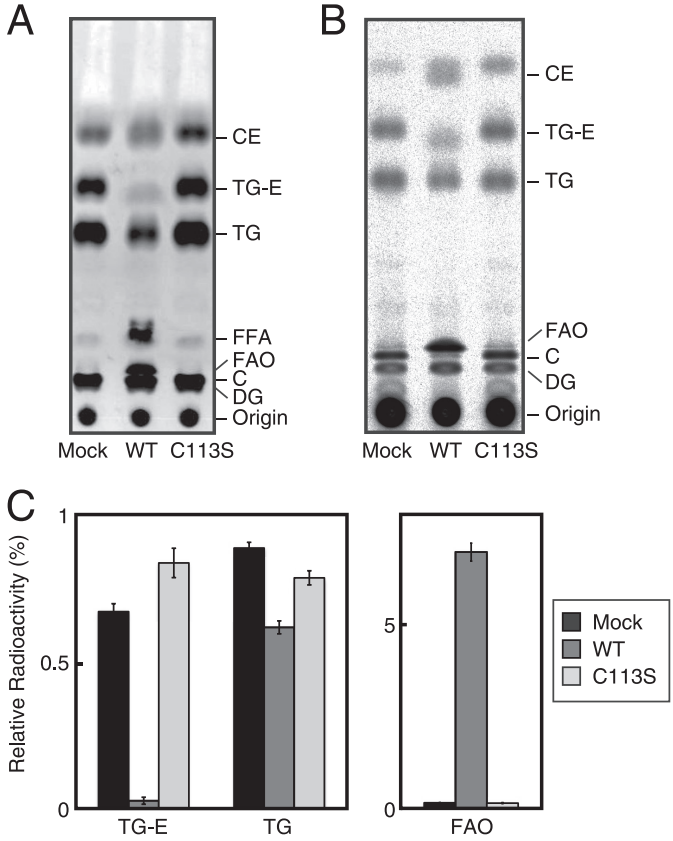

FIGURE 2. **Analysis of neutral lipids and free fatty acids in H-rev107/HEK293 and C113S/HEK293 cells.** *A*, total lipids were extracted from Mock/HEK293 (*Mock*), H-rev107/HEK293 (*WT*), and C113S/HEK293 (*C113S*) cells with acetone, as described under "Experimental Procedures," and were subjected to TLC analysis with solvent B. Lipids were visualized with primulin. The experiments were performed three times, and a representative result is shown. The positions of authentic compounds on the TLC plate are indicated. *CE*, cholesteryl ester; *FFA*, free fatty acid; *FAO*, free fatty alcohol; *C*, cholesterol; *DG*, diglyceride. *B* and *C*, cells were radiolabeled with [^{14}C]hexadecanol, and their total lipids were extracted and separated by TLC as described in *A*. Distribution of radioactivity on the TLC plate is shown (*B*). Relative radioactivities of TG-E, TG, and free fatty alcohol are shown (mean values ± S.D. (*error bars*), n = 3) (*C*). The experiments were performed three times, and a representative result is shown.

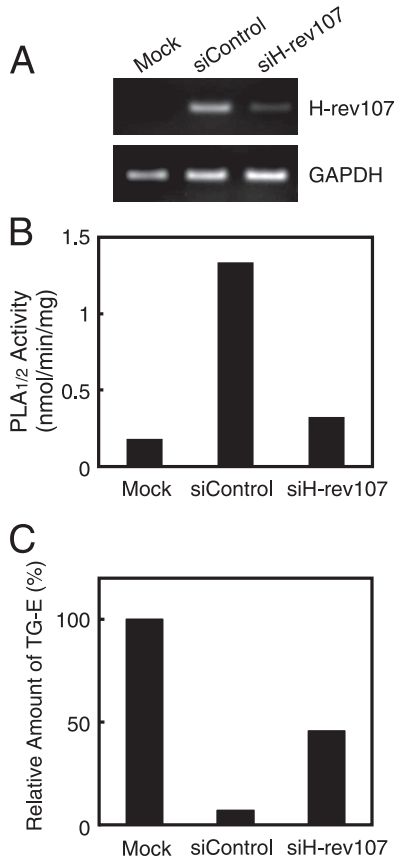

FIGURE 3. **Knockdown of *H-rev107* in H-rev107/HEK293 cells.** *A*, H-rev107/HEK293 cells were transfected with a control siRNA (*siControl*) or *H-rev107* siRNA (*siH-rev107*). After 48 h, total RNAs were isolated and analyzed by RT-PCR using specific primers for H-rev107 and GAPDH (a control). *Mock*, Mock/HEK293 cells. *B*, the cell homogenates (30 μg of protein) were subjected to the $PLA_{1/2}$ assay with 200 μM 1,2-[^{14}C]dipalmitoyl-PC as a substrate. *C*, after cells were radiolabeled with [^{14}C]hexadecanol, total lipids were extracted and separated by TLC with solvent B, and radioactive TG-E was quantified. TG-E level of Mock/HEK293 cells is normalized to 100%.

TLC, H-rev107/HEK293 cells exhibited strong radioactive bands corresponding to free palmitic acid and lyso-PC (Fig. 1*B*). The $PLA_{1/2}$ activity was estimated to be 1.36 nmol/min/mg of protein, which was 9.1-fold higher than that of a mock transfectant (Mock/HEK293 cell) (Fig. 1*C*). On the other hand, the $PLA_{1/2}$ activity of C113S/HEK293 cells was as low as that of Mock/HEK293 cells. Although *H-rev107* was originally found as a tumor suppressor gene regulating cell growth (3), the transfection of HEK293 cells with *H-rev107* or with the C113S mutant did not alter their growth rates, as examined by an MTT assay (Fig. 1*D*).

Examination of Lipid Profile—To clarify whether overexpression of H-rev107 affects the lipid profile of HEK293 cells, we extracted total lipids from the cells and separated them by TLC. In the assays shown in Fig. 2, we used solvent B, which is suitable for separation of various neutral lipids and free fatty acids. As visualized with primulin (Fig. 2*A*), H-rev107 enhanced bands that comigrated with authentic free fatty acid and free fatty alcohol as well as remarkably attenuated a band that comigrated with authentic TG-E. Identification of the bands as free fatty acid, free fatty alcohol, and TG-E was carried out by cochromatography with authentic compounds on TLC plates using two additional solvent systems ($CHCl_3$/acetone/acetic acid = 96:4:1 and $CHCl_3$/MeOH/H_2O = 65:25:4). These alterations of the lipid profile were not seen with C113S/HEK293 cells (Fig. 2*A*). We next metabolically labeled the cells with [^{14}C]hexadecanol as a representative fatty alcohol and separated the resultant radiolabeled lipid molecules by TLC. The results were in agreement with the aforementioned primulin staining. Namely, the expression of H-rev107 caused a reduction in radioactive TG-E by 96% and a concomitant 45-fold increase in free [^{14}C]hexadecanol (Fig. 2, *B* and *C*). Triacyl-type TG was decreased by 31%. Again, these alterations were not seen in C113S/HEK293 cells.

To confirm that these alterations were attributable to the expression of H-rev107 rather than the insertion of the *H-rev107* gene into a specific region of the genome that contains one or more genes related to the biosynthesis of ether-type lipids, we suppressed the expression of H-rev107 in H-rev107/HEK293 cells by transiently introducing siRNA against *H-rev107* (Fig. 3*A*). The suppression led to the partial recovery of endogenous TG-E levels as well as the reduction in $PLA_{1/2}$ activity of the cell homogenates (Fig. 3, *B* and *C*). In addition, we

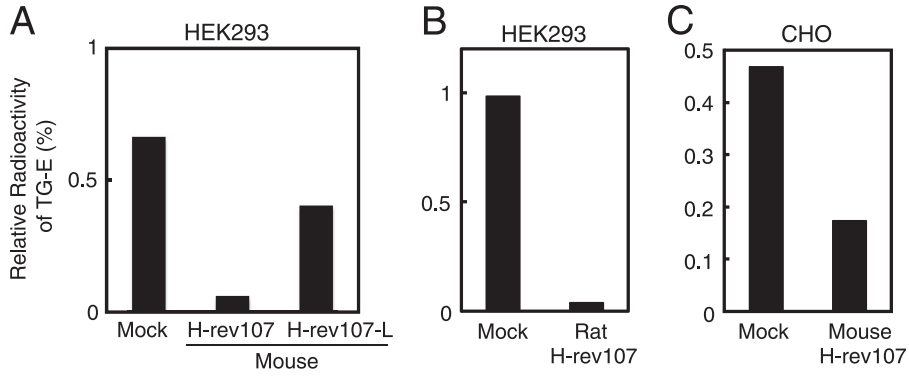

FIGURE 4. **Reduction in TG-E levels in H-rev107-expressing cells.** After cells were radiolabeled with [^{14}C]palmitic acid, total lipids were extracted and separated by TLC with solvent B, and radioactive TG-E was quantified. *A*, H-rev107/HEK293 and H-rev107-L/HEK293 cells, both of which expressed mouse H-rev107, were compared with Mock/HEK293. *B*, HEK293 cells expressing rat H-rev107 were compared with Mock/HEK293 cells. *C*, CHO cells expressing mouse H-rev107 were compared with Mock/CHO cells.

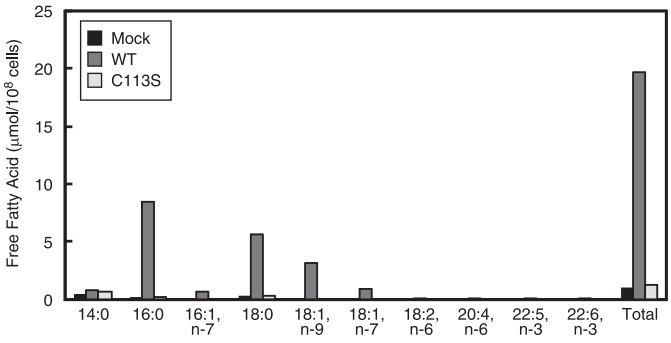

FIGURE 5. **Analysis of fatty acids by GC/MS.** Free fatty acids from Mock/HEK293 (*Mock*), H-rev107/HEK293 (*WT*), and C113S/HEK293 (*C113S*) cells were subjected to GC/MS after purification by TLC. Heptadecanoic acid (17:0) was used as an internal standard.

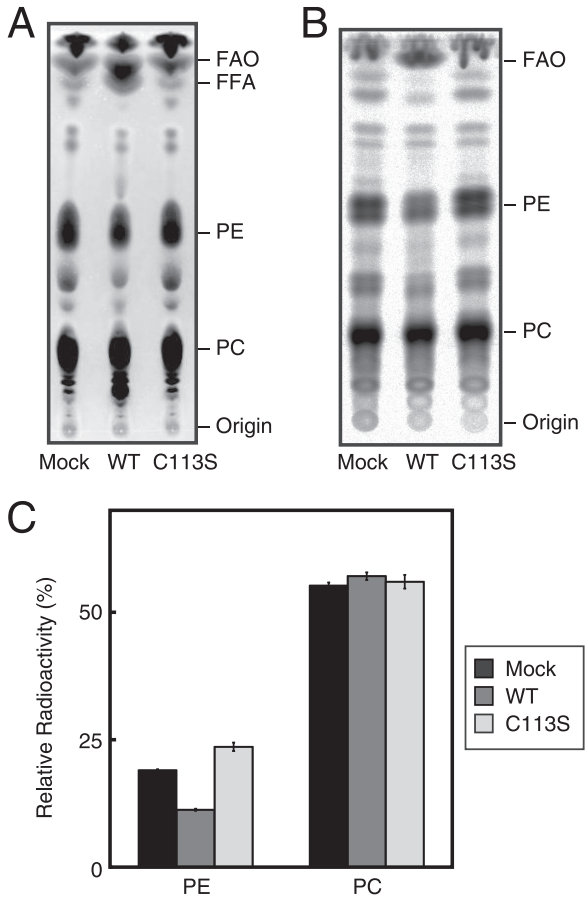

FIGURE 6. **Analysis of glycerophospholipids in H-rev107/HEK293 and C113S/HEK293 cells.** *A*, the total lipids were extracted from Mock/HEK293 (*Mock*), H-rev107/HEK293 (*WT*), and C113S/HEK293 (*C113S*) cells with acetone as described under "Experimental Procedures" and were subjected to TLC analysis with solvent A. Lipids were visualized with primulin. The experiments were performed three times, and a representative result is shown. The positions of authentic compounds on the TLC plate are indicated. *FAO*, free fatty alcohol; *FFA*, free fatty acid. *B* and *C*, cells were radiolabeled with [^{14}C]hexadecanol, and their total lipids were extracted and separated by TLC as described in *A*. Distribution of radioactivity on the TLC plate is shown (*B*). Relative radioactivities of PE and PC are shown (mean values ± S.D. (*error bars*), $n = 3$) (*C*). The experiments were performed three times, and a representative result is shown.

obtained another HEK293 cell clone stably expressing mouse H-rev107 (H-rev107-L/HEK293 cells), which, when homogenized, showed a lower $PLA_{1/2}$ activity (0.66 nmol/min/mg of protein). When Mock/HEK293, H-rev107/HEK293, and H-rev107-L/HEK293 cells were metabolically labeled with [^{14}C]palmitic acid for 18 h, the ratio of radioactive TG-E levels was 100:9:60 (Fig. 4*A*). To rule out the possibility that this change occurred only with a combination of mouse H-rev107 and HEK293 cells, we established two additional clones: a HEK293 cell clone stably expressing rat H-rev107 and a CHO cell clone stably expressing mouse H-rev107. These two cell lines also showed remarkable reductions in TG-E levels (Fig. 4, *B* and *C*). Taken together, these results strongly suggested that the enzyme activity of H-rev107 is responsible for the decrease in TG-E levels.

We also extracted free fatty acids from the corresponding band on the TLC plate and quantitated them by GC/MS (Fig. 5). Consistent with the result shown in Fig. 2*A*, the free fatty acid level was increased ~20-fold upon overexpression of the catalytically active H-rev107. The major species of the increased free fatty acids were saturated fatty acids (16:0 and 18:0) and monounsaturated fatty acids (18:1(*n*-9) and 18:1(*n*-7)), whereas the levels of polyunsaturated fatty acids, such as linoleic acid (18:2(*n*-6)) and arachidonic acid (20:4(*n*-6)), were very low. In contrast, the overexpression of the C113S mutant did not increase the levels of any free fatty acids.

We next analyzed phospholipids by TLC using solvent A (Fig. 6*A*). The band corresponding to PE from H-rev107/HEK293 cells appeared fainter than that from Mock/HEK293

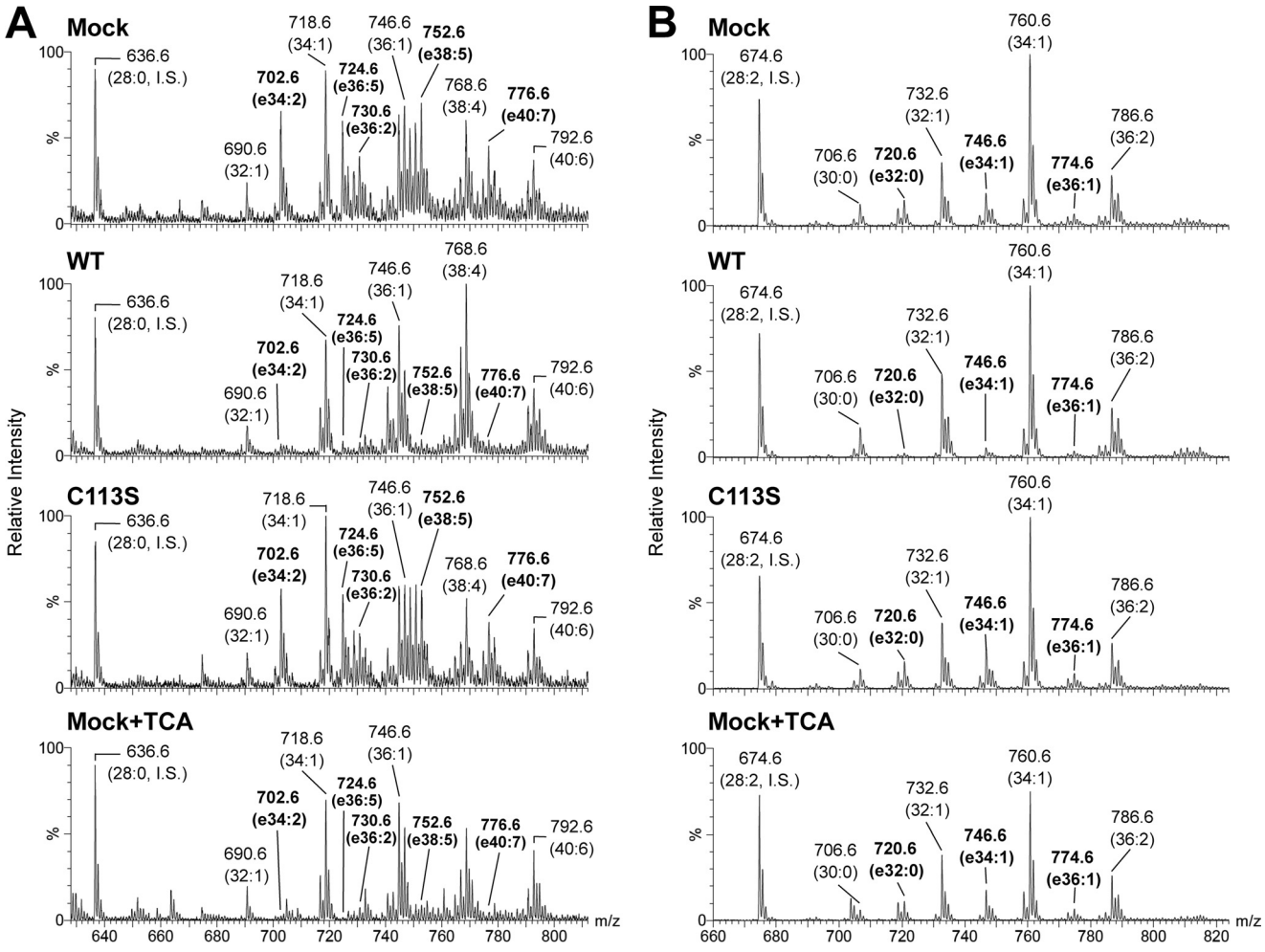

C

Phospholipid class	$[M+H]^+$ m/z	Molecular species
Ethanolamine phospholipid	702.6	p16:0/18:1, p18:0/16:1
Ethanolamine phospholipid	724.6	p16:0/20:4
Ethanolamine phospholipid	730.6	p18:0/18:1, p16:0/20:1
Ethanolamine phospholipid	752.6	p18:0/20:4, p16:0/22:4
Ethanolamine phospholipid	776.6	p18:0/22:6, p16:0/24:6
Choline phospholipid	720.6	a16:0/16:0
Choline phospholipid	746.6	a16:0/18:1
Choline phospholipid	774.6	a18:0/18:1

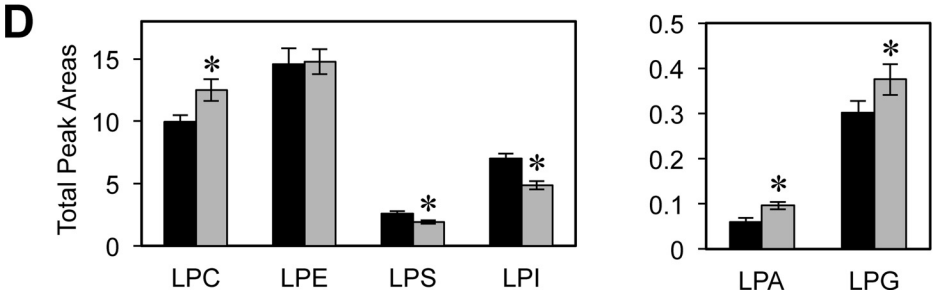

cells. We also analyzed radiolabeled phospholipids obtained by metabolic labeling with [^{14}C]hexadecanol (Fig. 6, *B* and *C*). The expression of H-rev107 decreased the radioactive PE level by 41%. Such a decrease in PE levels was not seen in C113S/HEK293 cells. The levels of radioactive PC were almost the same among all of the samples. To clarify which species of PE were decreased by the expression of H-rev107, we analyzed the extracted phospholipids by LC-ESI/MS. As shown in Fig. 7*A*, Mock/HEK293 cells contained various diacyl-type PE species (32:1, 34:1, 36:1, 38:4, and 40:6) and ether-type ethanolamine phospholipid species (e34:2, e36:2, e36:5, e38:5, and e40:7). Surprisingly, the expression of H-rev107 caused a specific and remarkable reduction in all of the ether-type ethanolamine phospholipid species. Similarly, the levels of ether-type choline phospholipids were decreased in H-rev107/HEK293 cells (Fig. 7*B*). The profiles of ethanolamine phospholipids and choline phospholipids in C113S/HEK293 cells were essentially the same as those of Mock/HEK293 cells. These results showed that the expression of H-rev107 decreases endogenous levels of ether-type glycerophospholipids as well as TG-E.

We further characterized molecular species of ether-type phospholipids. The vinyl ether linkage at the *sn*-1 position of phospholipids, such as plasmalogen, is known to be acid-labile (18). When Mock/HEK293 cells were treated with 5% TCA followed by total lipid extraction, the levels of ether-type ethanolamine phospholipid species were remarkably decreased, whereas diacyl-type PE and PC and ether-type choline phospholipids were hardly affected (Fig. 7, *A* and *B*). These results indicated that the observed ether-type ethanolamine and choline phospholipid species are principally plasmenylethanolamine and plasmanylcholine species, respectively.

We also performed product ion scanning of $[M - H]^-$ ions of ether-type ethanolamine phospholipids (Fig. 8*A*) and $[M + Li]^+$ ions of ether-type choline phospholipids (Fig. 8*C*) as described previously (19, 20). These analyses gave detailed information about molecular species of ether-type phospholipids, which was consistent with the results of acid treatment (Figs. 7*C* and 8, *B* and *D*).

Moreover, we analyzed endogenous levels of various lysophospholipids (Fig. 7*D*). H-rev107/HEK293 cells showed significantly higher levels of lyso-PC, lysophosphatidic acid, and lysophosphatidylglycerol than Mock/HEK293 cells, whereas the levels of lysophosphatidylserine and lysophosphatidylinositol were significantly lower. Lysophosphatidylethanolamine did not show a significant difference.

The selective reduction in ether-type lipids raised the possibility that these lipids serve as substrates of H-rev107. However, purified recombinant rat H-rev107 (6) could hardly hydrolyze plasmalogen-type ethanolamine phospholipid or TG-E (data not shown). This result suggested that the reduction in ether-type lipids is caused by one or more mechanisms different from direct degradation by H-rev107.

Analysis of Peroxisomal Proteins—The first two steps in the biosynthetic pathway of ether-type lipids occur in peroxisomes by dihydroxyacetone phosphate (DHAP) acyltransferase (DHAPAT) and alkyl-DHAP synthase (ADHAPS) (Fig. 9*A*) (21). DHAPAT transfers an acyl chain of acyl-CoA to DHAP, forming acyl-DHAP. ADHAPS replaces the esterified acyl chain of acyl-DHAP with a fatty alcohol, leading to the formation of alkyl-DHAP. Alkyl-DHAP is thought to be a common precursor for plasmalogen and TG-E. Therefore, dysfunction of these enzymes results in the impairment of ether-type lipid synthesis (21). Furthermore, the fatty acyl-CoA reductases Far 1 and Far 2 supply fatty alcohol used for the formation of ether-type lipids (22). Overexpression of H-rev107 or the C113S mutant did not appear to affect the expressions of DHAPAT, ADHAPS, Far 1, and Far 2 in HEK293 cells (Fig. 9*B*). PMP70 and catalase are known as marker proteins for peroxisomes. The expression levels of both mRNAs were also similar among Mock/HEK293, H-rev107/HEK293, and C113S/HEK293 cells (Fig. 9*B*).

We next analyzed subcellular localization of PMP70 and catalase proteins in these cells (Fig. 9*C*). For this purpose, we prepared three subcellular fractions (18,000 $\times$ *g* pellet as light mitochondrial fraction, 105,000 $\times$ *g* pellet as microsomal fraction, and 105,000 $\times$ *g* supernatant as cytosolic fraction) from cell homogenates by sequential centrifugations and further subjected the resultant light mitochondrial fractions, rich in peroxisomes, to discontinuous sucrose density gradient centrifugation. PMP70 and catalase proteins were enriched in fractions 4, 5, and 6 of Mock/HEK293 and C113S/HEK293 cells, whereas the corresponding fractions of H-rev107/HEK293 cells contained much lower levels of these proteins. Instead, catalase was mainly detected in the cytosolic fraction of H-rev107/HEK293 cells, suggesting the leakage of catalase into cytoplasm. On the other hand, PMP70 was not detected in any fractions of H-rev107/HEK293 cells. We also examined subcellular distribution of marker proteins for other organelles (syntaxin 6 for Golgi apparatus, protein-disulfide isomerase for ER, cytochrome *c* oxidase IV for mitochondrion, actin for cytosol, and lamin A/C for nucleus). The results showed that these marker proteins were localized in the expected fractions of all of the cells.

For morphological observations, H-rev107/HEK293 and Mock/HEK293 cells were transiently transfected with the expression vector harboring DsRed2-Peroxi, a fluorescent protein targeted to peroxisomes with the aid of peroxisomal targeting signal 1 (PTS1). When visualized by fluorescence microscopy, DsRed2-Peroxi exhibited the punctate structure characteristic of peroxisomes in Mock/HEK293 cells (Fig. 10*A*).

FIGURE 7. **Analysis of PE, PC, and lysophospholipids by LC-ESI/MS**. Total lipids were extracted from Mock/HEK293 (*Mock*), H-rev107/HEK293 (*WT*), C113S/HEK293 (*C113S*), and 5% TCA-treated Mock/HEK293 (*Mock + TCA*) cells by the Bligh and Dyer method. *A* and *B*, mass spectra of $[M + H]^+$ ions of ethanolamine phospholipids (*A*) and choline phospholipids (*B*) were detected by LC-ESI/MS. Dimyristoyl-PE (28:0) (*A*) and dimyristoleoyl-PC (28:2) (*B*) were used as internal standards. *C*, summary of molecular species of ether-type PE and PC determined by LC-ESI/MS/MS and acid lability. The prefixes "a" and "p" indicate a chain with an alkyl ether linkage and a chain with a vinyl ether linkage, respectively. *D*, total lipids were extracted from Mock/HEK293 (*black bar*) and H-rev107/HEK293 (*gray bar*) cells, and the indicated lysophospholipids were analyzed by LC-MS/MS. Mean values ± S.D. (*error bars*) are shown ($n = 5$). The *asterisks* indicate significant differences as compared with Mock/HEK293 cells ($p < 0.003$). *LPC*, lyso-PC; *LPE*, lyso-PE; *LPS*, lysophosphatidylserine; *LPI*, lysophosphatidylinositol; *LPA*, lysophosphatidic acid; *LPG*, lysophosphatidylglycerol.

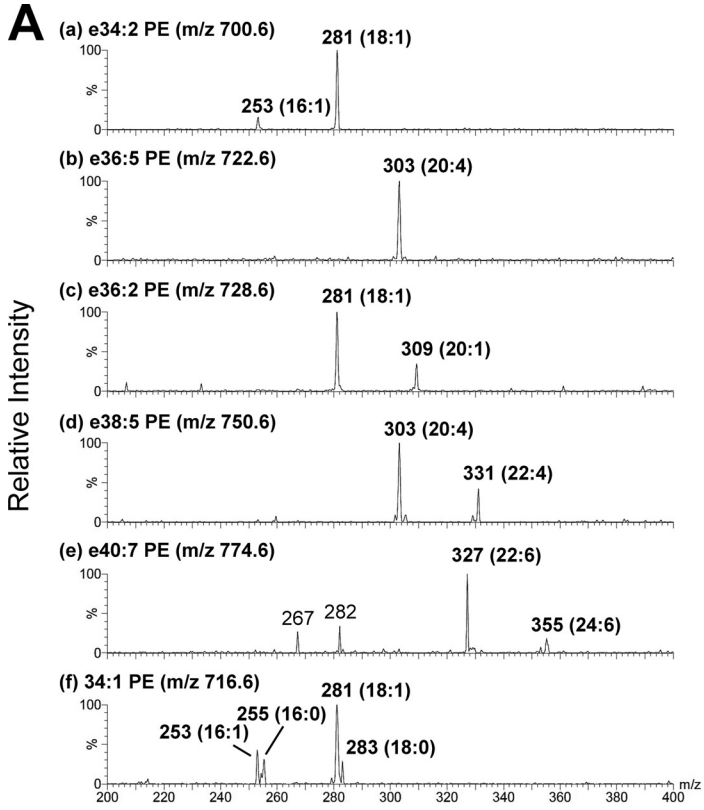

B

[M-H]$^-$ m/z	Molecular species
700.6	p16:0/18:1 PE, p18:0/16:1 PE
722.6	p16:0/20:4 PE
728.6	p18:0/18:1 PE, p16:0/20:1 PE
750.6	p18:0/20:4 PE, p16:0/22:4 PE
774.6	p18:0/22:6 PE, p16:0/24:6 PE
716.6	16:0/18:1 PE, 18:0/16:1 PE

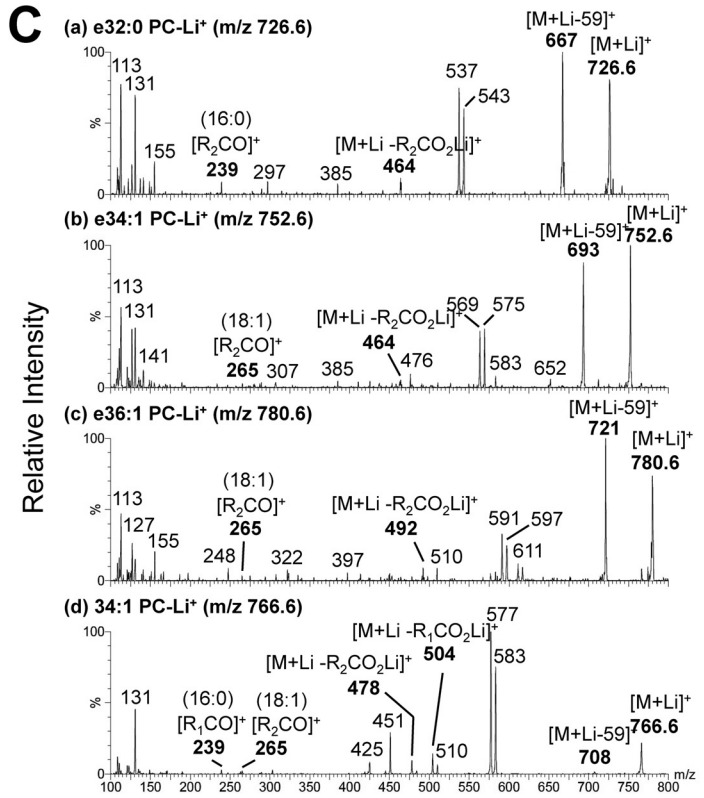

D

[M+Li]$^+$ m/z	Molecular species
726.6	a16:0/16:0 PC
752.6	a16:0/18:1 PC
780.6	a18:0/18:1 PC
766.6	16:0/18:1 PC

FIGURE 8. **Determination of molecular species of ether-type ethanolamine and choline phospholipids by product ion scanning.** *A*, the product ion spectra of the $[M - H]^-$ ions of the major ether-type ethanolamine phospholipids (*a*–*e*) and 34:1 PE (*f*) from Mock/HEK293 cells are shown. *C*, the product ion spectra of the $[M + Li]^+$ ions of the major ether-type choline phospholipids (*a*–*c*) and 34:1 PC (*d*) from Mock/HEK293 cells are shown. Note that the $[M + Li - 59]^+$ ion, which is characteristic of ether-type choline phospholipids, is prominent in the product ion spectra of *m/z* 726.6, 752.6, and 780.6. R_1CO- and R_2CO-, the *sn*-1 and *sn*-2 acyl chains, respectively, of phospholipids. *B* and *D*, molecular species determined by product ion scanning (*A* and *C*) and acid-lability (Fig. 7, *A* and *B*) are summarized. The prefixes "a" and "p" indicate a chain with an alkyl ether linkage and a chain with a vinyl ether linkage, respectively.

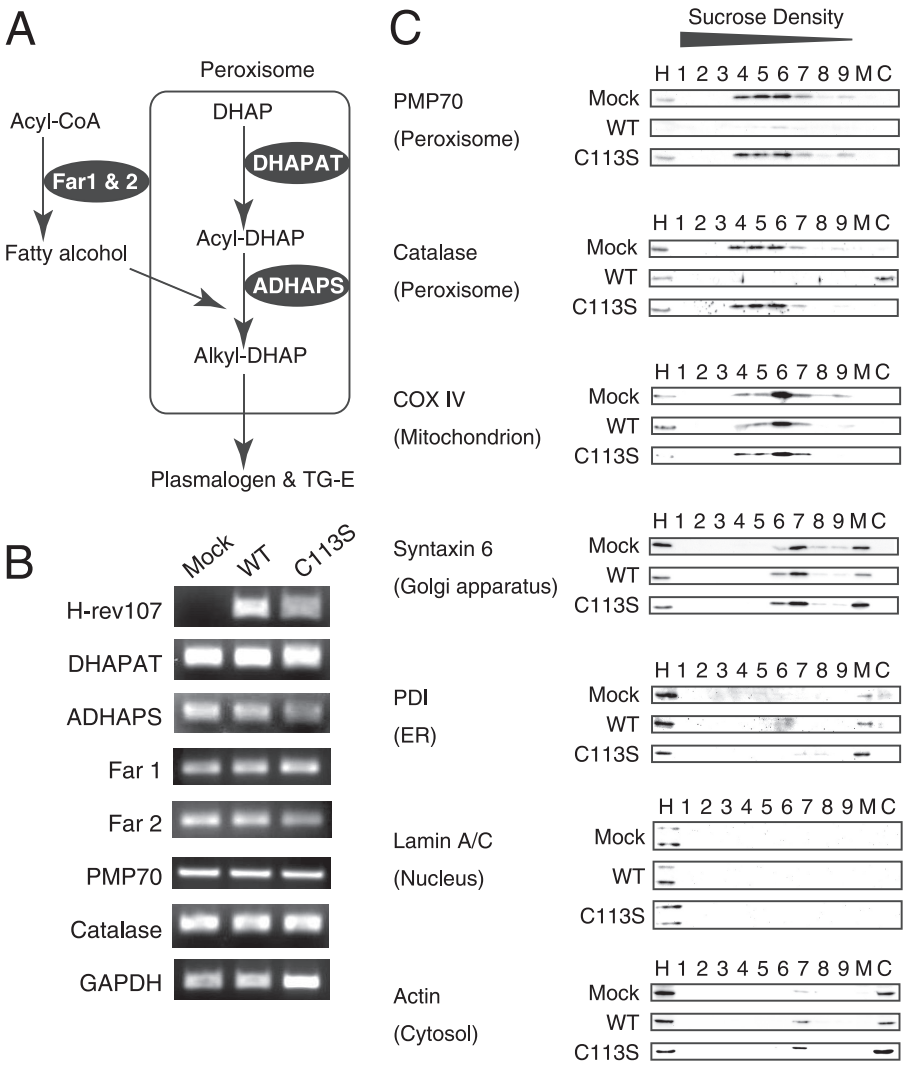

FIGURE 9. **Expression and subcellular distribution of peroxisomal proteins and ether-type lipid-biosynthesizing enzymes in H-rev107/HEK293 cells.** *A*, outline of the biosynthetic pathway of ether-type lipids. *B*, total RNAs were isolated from Mock/HEK293 (*Mock*), H-rev107/HEK293 (*WT*), and C113S/HEK293 (*C113S*) cells and analyzed by RT-PCR using specific primers for the indicated molecules. GAPDH was used as a control. *C*, the homogenates of Mock/HEK293, H-rev107/HEK293, and C113S/HEK293 cells were fractionated by sequential centrifugation at 3,000 × *g*, 18,000 × *g*, and 105,000 × *g*, and the 18,000 × *g* pellets (light mitochondrial fractions) were further subjected to discontinuous sucrose density gradient centrifugation as described under "Experimental Procedures." The homogenates (20 μg of protein in 20 μl) and each fraction (the corresponding volume to the homogenates) were analyzed by Western blotting with antibodies against the indicated proteins. *H*, *M*, and *C*, homogenate, microsomal fraction (105,000 × *g* pellet), and cytosolic fraction (105,000 × *g* supernatant), respectively. *COX IV*, cytochrome *c* oxidase IV; *PDI*, protein-disulfide isomerase.

However, DsRed2-Peroxi fluorescence was diffusely observed in the cytosol of H-rev107/HEK293 cells, and the peroxisome-like structures were absent (Fig. 10*A*). When PMP70 was immunostained, Mock/HEK293 cells revealed the punctate staining characteristic of peroxisomes, whereas such punctate structures of peroxisomes were not observed in H-rev107/HEK293 cells (Fig. 10*B*). Additionally, catalase was diffusely immunostained in H-rev107/HEK293 cells in contrast with the punctate staining in Mock/HEK293 cells (Fig. 10*C*). These results were consistent with the results of Western blotting shown in Fig. 9*C* and showed that the overexpression of H-rev107 alters intracellular localization of peroxisomal markers. The loss of PMP70 (23, 24) and the leakage of catalase into cytoplasm (25, 26) are reported in peroxisome deficiency.

Cellular Localization of H-rev107—Previously, H-rev107 fused to the N terminus of EGFP was transiently expressed in differentiated 3T3-L1 cells and was shown to exist in the ER and cytoplasm (10). To determine whether H-rev107 is also present in peroxisomes, we transiently expressed H-rev107 fused to the C terminus of EGFP (EGFP-H-rev107) in HEK293 cells. When analyzed by Western blotting with anti-GFP antibody, the cell homogenates exhibited two immunopositive bands at ~46 and ~27 kDa (Fig. 11*A*). Based on the deduced amino acid sequence of H-rev107 fused to EGFP, the ~46 kDa band corresponded to the whole fusion protein, whereas the ~27 kDa band was presumed to be a degradation product lacking the H-rev107 region. On the other hand, when EGFP-H-rev107 was transiently expressed in HeLa cells, such a degradation product was hardly detected (Fig. 11*A*). A similar result was obtained with H-rev107 fused to the N terminus of EGFP (Fig. 11*B*). Thus, we investigated the intracellular distribution of EGFP-H-rev107 in HeLa cells. When the homogenates of HeLa cells expressing EGFP-H-rev107 were subjected to ultracentrifugation at 105,000 × *g*, both the particulate and soluble fractions exhib-

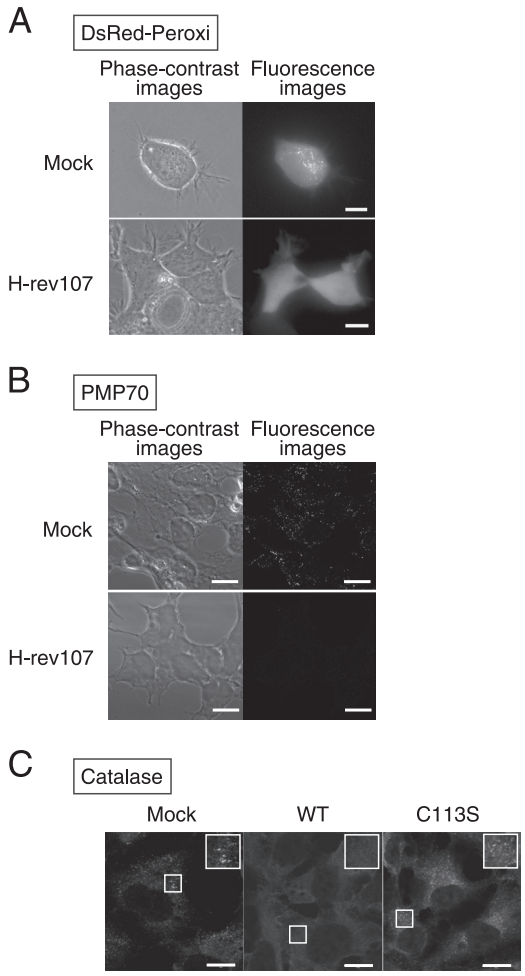

FIGURE 10. **Disappearance of peroxisomal structures from H-rev107/HEK293 cells.** *A*, Mock/HEK293 cells (*top panels*) and H-rev107/HEK293 cells (*bottom panels*) were cultured on glass slips, transiently transfected with the DsRed2-Peroxi-expressing vector, and observed with an epifluorescence microscope. Phase-contrast images (*left panels*) correspond to fluorescence images (*right panels*). *Scale bars*, 10 μm. *B*, Mock/HEK293 cells (*top panels*) and H-rev107/HEK293 cells (*bottom panels*) were immunostained with anti-PMP70 antibody and observed with a confocal laser-scanning microscope. Phase-contrast images (*left panels*) correspond to fluorescence images (*right panels*). *Scale bars*, 10 μm. *C*, Mock/HEK293 cells (*Mock*), H-rev107/HEK293 cells (*WT*), and C113S/HEK293 cells (*C113S*) were immunostained with anti-catalase antibody and observed with a confocal laser-scanning microscope. Areas enclosed with *squares* are magnified in *insets*. *Scale bars*, 10 μm.

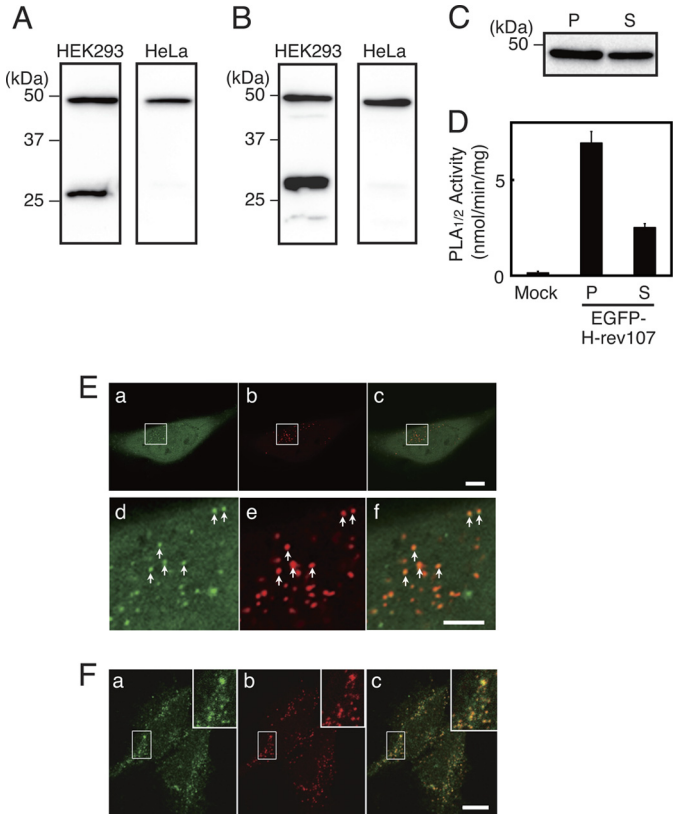

FIGURE 11. **Cellular localization of the transiently expressed H-rev107.** *A* and *B*, homogenates (10 μg of protein) of HEK293 and HeLa cells, both of which expressed H-rev107 fused to the C terminus of EGFP (EGFP-H-rev107) (*A*) or H-rev107 fused to the N terminus of EGFP (*B*), were analyzed by Western blotting with anti-GFP antibody. *C* and *D*, particulate (*P*) and soluble (*S*) fractions (10 μg of protein) were prepared from the homogenates of HeLa cells expressing EGFP-H-rev107 and were analyzed by Western blotting with anti-GFP antibody (*C*) or subjected to the $PLA_{1/2}$ assay with 200 μM 1,2-[^{14}C]dipalmitoyl-PC as a substrate (mean values $\pm$ S.D. (*error bars*), $n = 3$) (*D*). The $PLA_{1/2}$ activity of the homogenates of Mock/HeLa cells (*Mock*) (10 μg of protein) is also shown. *E*, HeLa cells were cultured on glass slips, transiently cotransfected with the EGFP-H-rev107-expressing vector and the DsRed2-Peroxi-expressing vector, and observed with a confocal laser-scanning microscope. Areas enclosed with *squares* in *a–c* are magnified in *d–f*, respectively. Images for EGFP-H-rev107 (*a* and *d*) and DsRed2-Peroxi (*b* and *e*) are merged in *c* and *f*. The *arrows* in *d–f* denote colocalization of EGFP-H-rev107 and DsRed2-Peroxi. *Scale bars*, 10 μm in *a–c* and 5 μm in *d–f*. *F*, HEK293 cells transiently expressing N-terminally FLAG-tagged H-rev107 and DsRed2-Peroxi were cultured on glass slips, immunostained with anti-H-rev107 antibody, and observed with a confocal laser-scanning microscope. Images for H-rev107 (*a*) and DsRed2-Peroxi (*b*) are merged in *c*. Areas enclosed with *squares* are magnified in *insets*. *Scale bars*, 10 μm.

ited the ~46 kDa immunopositive band as well as $PLA_{1/2}$ activity (Fig. 11, *C* and *D*). The enzyme activity of the particulate fraction was about 3-fold higher than that of the soluble fraction. In HeLa cells observed by confocal laser microscopy, EGFP-H-rev107 was distributed throughout the cytoplasm and nucleoplasm (Fig. 11*E*). The reticular pattern suggesting the presence in ER was not observed. Interestingly, in some of the observed cells, EGFP-H-rev107 appeared to be associated with peroxisomes, which were identified by the signal of DsRed2-Peroxi (*arrows* in Fig. 11*E*). Moreover, H-rev107 was transiently expressed in HEK293 cells together with DsRed2-Peroxi and immunostained with anti-H-rev107 antibody (Fig. 11*F*). Fluorescence microscopy revealed partial colocalization of H-rev107 with DsRed2-Peroxi, supporting the association of H-rev107 with peroxisomes.

DISCUSSION

We previously found that the tumor suppressor H-rev107 of humans, rats, and mice has $PLA_{1/2}$ activity (6). Later we showed that the protein also possesses PE *N*-acyltransferase and lysophospholipid *O*-acyltransferase activities (7). Duncan *et al.* (10) also reported that H-rev107 acts as PLA_2. Similarly, other members of the HRASLS family (Ca^{2+}-independent *N*-acyltransferase, TIG3, and HRASLS2) exhibited phospholipid-metabolizing activities (8, 9). To reveal the intracellular function of H-rev107, in the present study, we successfully established HEK293 cells constitutively expressing H-rev107 (H-rev107/HEK293 cells). The expression of H-rev107 resulted in a considerable accumulation of free fatty acids, indicating that H-rev107 functions as a $PLA_{1/2}$ enzyme in the cells. Lysophos-

pholipid is another product of $PLA_{1/2}$. The endogenous levels of some classes of lysophospholipids were increased, whereas those of other classes were not. The results may be explained by a rapid turnover of lysophospholipids. More interestingly, we found that the stable expression of H-rev107 caused a strong decrease in ether-type lipids, such as plasmalogen and TG-E, with a concomitant accumulation of fatty alcohols necessary for the formation of ether-type lipids. Furthermore, we observed unusual localization or absence of peroxisomal markers. These phenotypes were not observed in HEK293 cells expressing a catalytically inactive mutant (C113S) of H-rev107, indicating that the lipid-metabolizing activity of H-rev107 is involved in these biochemical and morphological abnormalities. Because peroxisomes play important roles in the biosynthesis of ether-type lipids (21, 25–27) and because the decrease in the ether lipid level is caused by congenital deficiency of proteins involved in peroxisome biogenesis (28–30), our results suggest that the remarkable decrease in the ether-type lipid levels by the overexpression of H-rev107 might be due to the dysfunction of peroxisomes.

Two types of peroxisomal dysfunction impair the biosynthesis of ether-type lipids (21). One type of dysfunction is caused by defects in the peroxisomal enzymes DHAPAT and ADHAPS, which catalyze the first and second steps in the biosynthesis of ether-type lipids, respectively (25, 26). This abnormality does not affect the structure of peroxisomes. The other is caused by a defect in one of the *PEX* genes, which causes disappearance of peroxisomes (21, 31). So far, 32 peroxins have been found to be encoded by *PEX* genes (32). These proteins are involved not only in the biogenesis, proliferation, and division of peroxisomes but also in the targeting and import of peroxisomal proteins (33). The dysfunction is related to peroxisome biogenesis disorders, such as Zellweger syndrome and rhizomelic chondrodysplasia punctata (28). The phenotype of H-rev107/HEK293 cells is similar to that of the cells with a defect in *PEX* genes because the cells showed abnormal localization of the peroxisomal proteins, catalase and PMP70, despite normal expression levels of DHAPAT and ADHAPS mRNAs.

To elucidate the subcellular localization of H-rev107, we constructed a ~46-kDa fusion protein composed of H-rev107 and EGFP. However, the fusion protein was significantly degraded into a ~27-kDa protein when transiently expressed in HEK293 cells. Because such a proteolytic degradation did not occur in HeLa cells, we used the cells for further experiments. The fusion protein transiently expressed in HeLa cells was found to exist in both the particulate and soluble fractions, and its $PLA_{1/2}$ activity was also detectable in both fractions. We previously reported a similar distribution pattern with FLAG-tagged H-rev107 transiently expressed in COS-7 cells (6). Although the C-terminal hydrophobic domain of H-rev107 is required for membrane association (4, 10) and H-rev107 fused to the N terminus of EGFP was cytochemically localized in both ER and cytoplasm of differentiated 3T3-L1 cells (10), it was unclear from these studies whether H-rev107 was present in peroxisomes. Our microscopic observation revealed that H-rev107 fused to the C terminus of EGFP is in part localized in peroxisomes despite its lack of typical PTSs, such as C-terminal PTS1 and N-terminal PTS2 (32). Partial localization of H-rev107 in peroxisomes was further supported by the immunocytochemical observation with anti-H-rev107 antibody. These results suggest that H-rev107 can attach to peroxisomal membranes and degrade their phospholipids to free fatty acids and lysophospholipids by its catalytic activity. This damage of the membranes may cause abnormality of peroxisomes directly or through dysfunction of peroxisomal proteins, such as peroxins. However, further studies are needed to elucidate the mechanism by which peroxisomes are specifically impaired by the expression of H-rev107.

H-rev107 is highly expressed in adipose tissue (7, 10–12), and its expression is markedly up-regulated during the progression of adipogenesis (11, 12). Stimulation of peroxisome proliferator-activated receptor γ resulted in the induction of H-rev107 (12). Plasmalogen levels in white adipose tissues are much lower in genetically obese *ob/ob* mice than in wild-type mice (34). Furthermore, the TG-E level was high in undifferentiated 3T3-L1 cells but greatly reduced after their differentiation to adipocyte-like cells (35). The levels of ether-type lipids thus appear to be inversely correlated with the expression level of H-rev107. These previous findings may be partly explained by our present finding that H-rev107 expression decreases the levels of ether-type lipids.

In addition to the biosynthesis of ether-type lipids, peroxisomes are involved in the metabolism of a variety of lipids and other essential biomolecules, such as the degradation of very long-chain fatty acids, detoxification of hydrogen peroxide, and purine degradation (36). Moreover, it was recently demonstrated that generation of alkyl-containing glycosylphosphatidylinositol, the lipid portion of mammalian glycosylphosphatidylinositol-anchored proteins, is dependent upon the peroxisomal alkyl-phospholipid biosynthetic pathway (37). It may be interesting to investigate whether the expression of H-rev107 also affects these metabolic pathways in peroxisomes.

In summary, our results indicated that the enzyme activity of H-rev107 decreased intracellular levels of ether-type lipids and caused abnormality of peroxisomes in H-rev107/HEK293 cells. The accumulation of free fatty acids suggests that H-rev107 functions as a $PLA_{1/2}$ in living cells. Thus, in addition to functioning as a tumor suppressor and a regulator of adipocyte lipolysis, H-rev107 may regulate peroxisomal metabolism. It will be of interest to determine whether HRASLS family members other than H-rev107 possess similar biological activities.

Acknowledgments—We are grateful to Akiko Yamamoto and Yumi Tani for technical assistance. We also acknowledge technical assistance from the Division of Research Instrument and Equipment and Division of Radioisotope Research, Kagawa University.

REFERENCES

1. Shyu, R. Y., Hsieh, Y. C., Tsai, F. M., Wu, C. C., and Jiang, S. Y. (2008) Cloning and functional characterization of the HRASLS2 gene. *Amino acids* **35,** 129–137
2. Ueda, N., Tsuboi, K., and Uyama, T. (2010) Enzymological studies on the biosynthesis of *N*-acylethanolamines. *Biochim. Biophys. Acta* **1801,** 1274–1285
3. Hajnal, A., Klemenz, R., and Schäfer, R. (1994) Subtraction cloning of H-rev107, a gene specifically expressed in H-ras-resistant fibroblasts. *Oncogene* **9,** 479–490

4. Sers, C., Emmenegger, U., Husmann, K., Bucher, K., Andres, A. C., and Schäfer, R. (1997) Growth-inhibitory activity and down-regulation of the class II tumor-suppressor gene H-rev107 in tumor cell lines and experimental tumors. *J. Cell Biol.* **136,** 935–944
5. Lotz, K., Kellner, T., Heitmann, M., Nazarenko, I., Noske, A., Malek, A., Gontarewicz, A., Schäfer, R., and Sers, C. (2005) Suppression of the TIG3 tumor suppressor gene in human ovarian carcinomas is mediated via mitogen-activated kinase-dependent and -independent mechanisms. *Int. J. Cancer* **116,** 894–902
6. Uyama, T., Morishita, J., Jin, X. H., Okamoto, Y., Tsuboi, K., and Ueda, N. (2009) The tumor suppressor gene H-Rev107 functions as a novel Ca^{2+}-independent cytosolic phospholipase $A_{1/2}$ of the thiol hydrolase type. *J. Lipid Res.* **50,** 685–693
7. Uyama, T., Jin, X. H., Tsuboi, K., Tonai, T., and Ueda, N. (2009) Characterization of the human tumor suppressors TIG3 and HRASLS2 as phospholipid-metabolizing enzymes. *Biochim. Biophys. Acta* **1791,** 1114–1124
8. Jin, X. H., Okamoto, Y., Morishita, J., Tsuboi, K., Tonai, T., and Ueda, N. (2007) Discovery and characterization of a Ca^{2+}-independent phosphatidylethanolamine *N*-acyltransferase generating the anandamide precursor and its congeners. *J. Biol. Chem.* **282,** 3614–3623
9. Jin, X. H., Uyama, T., Wang, J., Okamoto, Y., Tonai, T., and Ueda, N. (2009) cDNA cloning and characterization of human and mouse Ca^{2+}-independent phosphatidylethanolamine *N*-acyltransferases. *Biochim. Biophys. Acta* **1791,** 32–38
10. Duncan, R. E., Sarkadi-Nagy, E., Jaworski, K., Ahmadian, M., and Sul, H. S. (2008) Identification and functional characterization of adipose-specific phospholipase A_2 (AdPLA). *J. Biol. Chem.* **283,** 25428–25436
11. Jaworski, K., Ahmadian, M., Duncan, R. E., Sarkadi-Nagy, E., Varady, K. A., Hellerstein, M. K., Lee, H. Y., Samuel, V. T., Shulman, G. I., Kim, K. H., de Val, S., Kang, C., and Sul, H. S. (2009) AdPLA ablation increases lipolysis and prevents obesity induced by high-fat feeding or leptin deficiency. *Nat. Med.* **15,** 159–168
12. Hummasti, S., Hong, C., Bensinger, S. J., and Tontonoz, P. (2008) HRASLS3 is a PPARγ-selective target gene that promotes adipocyte differentiation. *J. Lipid Res.* **49,** 2535–2544
13. Osumi, T., and Hashimoto, T. (1978) Enhancement of fatty acyl-CoA oxidizing activity in rat liver peroxisomes by di-(2-ethylhexyl)phthalate. *J. Biochem.* **83,** 1361–1365
14. Bligh, E. G., and Dyer, W. J. (1959) A rapid method of total lipid extraction and purification. *Can. J. Biochem. Physiol.* **37,** 911–917
15. Lee, H. C., Inoue, T., Imae, R., Kono, N., Shirae, S., Matsuda, S., Gengyo-Ando, K., Mitani, S., and Arai, H. (2008) *Caenorhabditis elegans mboa-7*, a member of the MBOAT family, is required for selective incorporation of polyunsaturated fatty acids into phosphatidylinositol. *Mol. Biol. Cell* **19,** 1174–1184
16. Araki, N., Hatae, T., Furukawa, A., and Swanson, J. A. (2003) Phosphoinositide-3-kinase-independent contractile activities associated with Fcγ-receptor-mediated phagocytosis and macropinocytosis in macrophages. *J. Cell Sci.* **116,** 247–257
17. Ren, X., Lin, J., Jin, C., and Xia, B. (2010) Solution structure of the N-terminal catalytic domain of human H-REV107. A novel circular permutated NlpC/P60 domain. *FEBS Lett.* **584,** 4222–4226
18. Honsho, M., Yagita, Y., Kinoshita, N., and Fujiki, Y. (2008) Isolation and characterization of mutant animal cell line defective in alkyl-dihydroxyacetonephosphate synthase. Localization and transport of plasmalogens to post-Golgi compartments. *Biochim. Biophys. Acta* **1783,** 1857–1865
19. Kerwin, J. L., Tuininga, A. R., and Ericsson, L. H. (1994) Identification of molecular species of glycerophospholipids and sphingomyelin using electrospray mass spectrometry. *J. Lipid Res.* **35,** 1102–1114
20. Hsu, F. F., Turk, J., Thukkani, A. K., Messner, M. C., Wildsmith, K. R., and Ford, D. A. (2003) Characterization of alkylacyl, alk-1-enylacyl, and lyso subclasses of glycerophosphocholine by tandem quadrupole mass spectrometry with electrospray ionization. *J. Mass Spectrom.* **38,** 752–763
21. Wanders, R. J., and Waterham, H. R. (2006) Biochemistry of mammalian peroxisomes revisited. *Annu. Rev. Biochem.* **75,** 295–332
22. Honsho, M., Asaoku, S., and Fujiki, Y. (2010) Posttranslational regulation of fatty acyl-CoA reductase 1, Far1, controls ether glycerophospholipid synthesis. *J. Biol. Chem.* **285,** 8537–8542
23. Yamasaki, M., Hashiguchi, N., Fujiwara, C., Imanaka, T., Tsukamoto, T., and Osumi, T. (1999) Formation of peroxisomes from peroxisomal ghosts in a peroxisome-deficient mammalian cell mutant upon complementation by protein microinjection. *J. Biol. Chem.* **274,** 35293–35296
24. South, S. T., and Gould, S. J. (1999) Peroxisome synthesis in the absence of preexisting peroxisomes. *J. Cell Biol.* **144,** 255–266
25. Nagan, N., Hajra, A. K., Larkins, L. K., Lazarow, P., Purdue, P. E., Rizzo, W. B., and Zoeller, R. A. (1998) Isolation of a Chinese hamster fibroblast variant defective in dihydroxyacetonephosphate acyltransferase activity and plasmalogen biosynthesis. Use of a novel two-step selection protocol. *Biochem. J.* **332,** 273–279
26. Nagan, N., Hajra, A. K., Das, A. K., Moser, H. W., Moser, A., Lazarow, P., Purdue, P. E., and Zoeller, R. A. (1997) A fibroblast cell line defective in alkyl-dihydroxyacetone phosphate synthase. A novel defect in plasmalogen biosynthesis. *Proc. Natl. Acad. Sci. U.S.A.* **94,** 4475–4480
27. Nagan, N., and Zoeller, R. A. (2001) Plasmalogens: biosynthesis and functions. *Prog. Lipid Res.* **40,** 199–229
28. Weller, S., Gould, S. J., and Valle, D. (2003) Peroxisome biogenesis disorders. *Annu. Rev. Genomics Hum. Genet.* **4,** 165–211
29. Steinberg, S. J., Dodt, G., Raymond, G. V., Braverman, N. E., Moser, A. B., and Moser, H. W. (2006) Peroxisome biogenesis disorders. *Biochim. Biophys. Acta* **1763,** 1733–1748
30. Van Veldhoven, P. P. (2010) Biochemistry and genetics of inherited disorders of peroxisomal fatty acid metabolism. *J. Lipid Res.* **51,** 2863–2895
31. Fujiki, Y., Okumoto, K., Kinoshita, N., and Ghaedi, K. (2006) Lessons from peroxisome-deficient Chinese hamster ovary (CHO) cell mutants. *Biochim. Biophys. Acta* **1763,** 1374–1381
32. Girzalsky, W., Saffian, D., and Erdmann, R. (2010) Peroxisomal protein translocation. *Biochim. Biophys. Acta* **1803,** 724–731
33. Yan, M., Rayapuram, N., and Subramani, S. (2005) The control of peroxisome number and size during division and proliferation. *Curr. Opin. Cell Biol.* **17,** 376–383
34. Medina-Gomez, G., Gray, S. L., Yetukuri, L., Shimomura, K., Virtue, S., Campbell, M., Curtis, R. K., Jimenez-Linan, M., Blount, M., Yeo, G. S., Lopez, M., Seppänen-Laakso, T., Ashcroft, F. M., Oresic, M., and Vidal-Puig, A. (2007) PPAR γ 2 prevents lipotoxicity by controlling adipose tissue expandability and peripheral lipid metabolism. *PLOS Genet.* **3,** e64
35. Bartz, R., Li, W. H., Venables, B., Zehmer, J. K., Roth, M. R., Welti, R., Anderson, R. G., Liu, P., and Chapman, K. D. (2007) Lipidomics reveals that adiposomes store ether lipids and mediate phospholipid traffic. *J. Lipid Res.* **48,** 837–847
36. Islinger, M., Cardoso, M. J., and Schrader, M. (2010) Be different. The diversity of peroxisomes in the animal kingdom. *Biochim. Biophys. Acta* **1803,** 881–897
37. Kanzawa, N., Maeda, Y., Ogiso, H., Murakami, Y., Taguchi, R., and Kinoshita, T. (2009) Peroxisome dependency of alkyl-containing GPI-anchor biosynthesis in the endoplasmic reticulum. *Proc. Natl. Acad. Sci. U.S.A.* **106,** 17711–17716